Photonic properties of ZnO epilayers

M. R. Wagner*[a], U. Haboeck[a], P. Zimmer[a], A. Hoffmann[a]
S. Lautenschläger[b], C. Neumann[b], J. Sann[b], B. K. Meyer[b]
[a]Institut für Festkörperphysik, Technische Universität Berlin, Hardenbergstr. 36, 10623 Berlin, Germany;
[b]I. Physikalisches Institut, Justus Liebig Universität Giessen, Heinrich-Buff-Ring 16, 35392 Gießen, Germany

ABSTRACT

The characterization by various experimental techniques of homoepitaxial growth and photonic properties of ZnO epilayers was exhaustively analyzed. The photonic properties of ZnO as promising material for the realization of polariton lasers were investigated by angular dependent reflection spectroscopy. The fitting of the polariton dispersion curve with the experimental results provided us information about the longitudinal-transverse exciton-polariton splitting and damping constants. In addition, the valence band symmetry was examined by angular resolved magneto-optical photoluminescence. From our theoretical and experimental results we extracted evidence that the topmost A valence band possesses Γ_7 symmetry. Micro-Raman spectroscopy revealed even in homoepitaxially grown samples the existence of compressive or tensile strain which varied not only in the ZnO layers but also in the templates. In contrast, the untreated substrates were uniformly strained. Sporadically crystal perturbations culminating in the formation of separated growth domains were observed. Additionally, resonant Raman scattering was performed, showing a strong enhancement of the $2E_1(LO)$ mode for resonant excitation of the I_8 bound exciton complex. We suggest that the resonant Raman scattering led to a longer lifetime of the resonantly excited phonon mode due to a strong exciton-phonon interaction.

Keywords: polariton laser, homoepitaxy, reflection spectroscopy, resonant Raman scattering, valence band structure, magneto-optical photoluminescence, time-resolved spectroscopy.

1. INTRODUCTION

Zinc oxide is a direct II-VI semiconductor that crystallizes in a wurtzite structure with a free exciton binding energy of 60meV [1, 2]. The large exciton binding energy leads to stable excitons at room temperature with large oscillator strength. Due to the bandgap energy of 3.37eV at 300K, the excitons emit blue to UV light during recombination. These properties make ZnO a highly promising candidate for the fabrication of coherent and monochromatic light sources at room temperature called polariton lasers. Polariton lasers require semiconductor micro-cavity structures with stable excitons, where the coherent light amplification is enabled by Bose condensation of exciton-polaritons in the confined structures. Recent publications underline the great potential of ZnO as material for polariton laser due to an extremely strong light-matter coupling and the advances in achieving p-type ZnO [3, 4]. However, the latter still poses a challenge.

One basic precondition is to reduce the n-type background carrier concentration of the source material, nominally undoped ZnO. Apart from avoiding the incorporation of impurities which can act as additional donors, the crystal quality must be improved to minimize defect-induced enhancement of free carriers or the generation of internal electric fields. Heteroepitaxial growth is frequently known to produce strained material arising from lattice and thermal mismatch. Such difficulties are not expected for a homoepitaxial growth since substrate and sample have the same lattice constants and thermal expanding coefficients. Raman spectroscopy is a common tool to probe crystal quality and strain properties.

In addition to micro-Raman spectroscopy, resonant Raman scattering was performed. The enhancement of the Raman scattering cross section can be observed when the energy of the incoming or scattered light corresponds to the energy of allowed optical transitions in the material.

*markus.wagner@physik.tu-berlin.de

Zinc Oxide Materials and Devices II, edited by Ferechteh Hosseini Teherani, Cole W. Litton,
Proc. of SPIE Vol. 6474, 64740X, (2007) · 0277-786X/07/$18 · doi: 10.1117/12.717785

The first theoretical descriptions of Resonant Raman Scattering (RRS) were given by Loudon in 1963 [5], while a more comprehensive theory was proposed by Ganguly and Birman in 1967 [6] and for RRS in ZnO by Calleja and Cardona in 1977 [7]. The early availability of high quality CdS crystals in the late 60ths resulted in extensive experimental studies of RRS in II-VI semiconductors [8-11]. However for ZnO, only a few publications concerning RRS on free and bound excitons are available.

Multiphonon Raman scattering has been reported for bulk ZnO [12], thin films [13], and nanostructures [14] although it should be noted, that the excitation was performed by a HeCd laser with an emission wavelength of 325nm and therefore far off the excitonic resonance in ZnO. There are some reports on RRS in ZnO layers and nanostructures excited by an Ar^+- laser with emission lines at 351nm and 364nm [15, 16]. These values are considerably closer to the bandgap energy of 3.437eV for ZnO at 4.2 Kelvin, compared to the excitation with a HeCd laser. However, the resonance behavior in the range of the free and bound exciton transitions can only be investigated for a fixed excitation wavelength if temperature dependent measurements are performed. This temperature variation leads to a shift of the absorption edge and therefore also affects the intensity of luminescence and Raman peaks. Obviously, the temperature influence on the intensity complicates a quantitative analysis of the resonance enhancement. Consequently, a tunable excitation source in the blue and near UV range is required to investigate the RRS in ZnO.

We start our survey on ZnO with a discussion of the band structure, namely the symmetry of the valence bands. From reflection spectroscopy investigations we deduce the dispersion relation of the exciton-polaritons and from magneto optical photoluminescence we draw conclusions on the valence band ordering. Finally we present the results of the Raman measurements mentioned above.

2. VALENCE BAND STRUCTURE AND MAGNETO OPTICAL PROPERTIES

The valence band of ZnO, which has a p-like wavefunction at the Γ-Point, is split due to the crystal field and spin-orbit interaction into three two-fold degenerated subbands which are labeled A, B, and C from the highest to the lowest band. Fig. 1 shows a schematic model of the valence band structure at the Γ-Point with a splitting of 4.9meV between the A and B valence band and 43.7meV between the B and C valence band at 4.2 Kelvin. The ordering of the valence bands, however, has been a subject of extensive discussions [2, 17-20] since the first investigations of the valence-band maximum fine structure by Thomas in 1960 [17]. Thomas came to the conclusion that the symmetry of the valence bands from the A, B, and C band is Γ_7, Γ_9, Γ_7 rather than, Γ_9, Γ_7, Γ_7 and therefore anomalous compared to the usual ordering in other wurtzite II-VI materials like ZnSe and CdS.

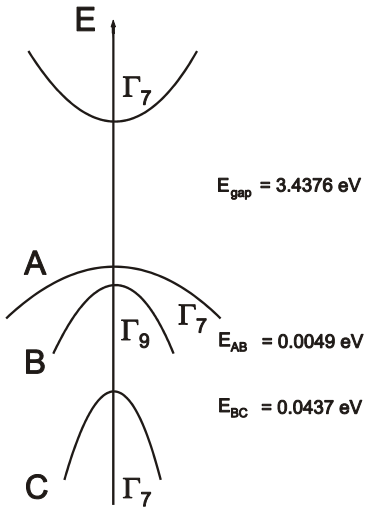

Fig. 1. Splitting of the valence band into the A, B, and C sub-bands with Γ_7, Γ_9, Γ_7 symmetry caused by the combined effects of crystal-field splitting and spin-orbit coupling. The energy values are indicated for T = 4.2 K.

Theoretical calculations within the framework of the local density approximation explain the reversed order of the top valence bands by a negative effective spin-orbit coupling. Such a negative splitting was first discussed in copper and silver halides by Cardona [21], while Shindo et al. [22] explained it by lower-lying d-bands and calculated a value of -8.7meV for the negative spin-orbit coupling. More recent calculations ascribed the negative spin-orbit coupling to the contribution of 7eV below the valence band lying Zn 3d bands [23].

An excellent experimental technique to investigate band structure properties is the reflection spectroscopy. In order to obtain a consistent image for different k-vectors, reflection spectra for various angles between the c-axis of the sample and the k-vector of the exciting light were conducted. Fig. 2 displays the angular dependent reflection spectra of ZnO for the exemplary angles of 10, 30 and 50 degree. The solid lines are the experimental recorded spectra, while the dashed lines represent the calculated spectra using a damped oscillator model. Fitting of the experimental data delivers values of $\omega_{LT,A}$=3.9eV and $\omega_{LT,B}$=9.0eV for the longitudinal-transverse splitting of the A and B exciton-polaritons. The transition energies were obtained to be E_A=3.3768eV and E_B=3.3815eV. The damping constants, which indicate the level of impurity incorporations, were determined to be $\Gamma_A=5\cdot10^{-5}$ and $\Gamma_B=8\cdot10^{-4}$.

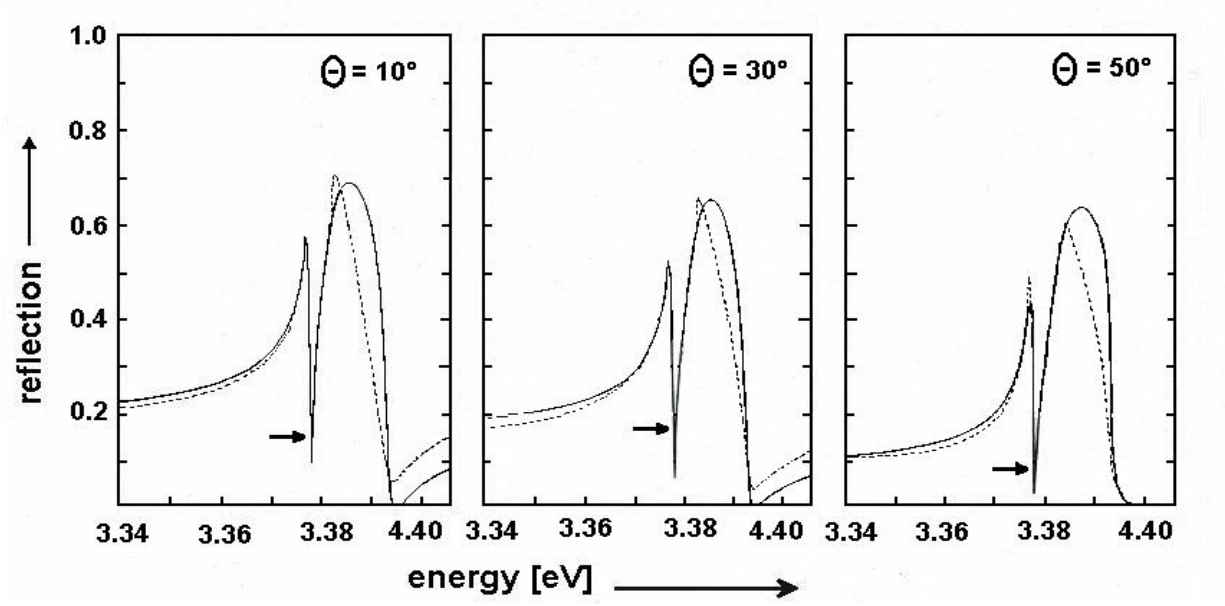

Fig. 2. Reflection spectra at 2 K of high-quality ZnO crystals. The reflectivity is depicted as a function of the excitation energy for angles of 10°, 30° and 50° between the crystal c-axis and the k-vector of the incident light. Solid lines and dashed lines represent the experimental and fitted curves, respectively.

From the angular dependent reflection spectra, the dispersion relation of the polaritons can be determined which are shown in Fig 3. Due to the interaction between the A and B exciton-polariton, the lowest branch of the B and the highest branch of the A exciton are strongly coupled. This has a significant influence on the selection rules for optical transitions. Usually, the $\Gamma_7 \rightarrow \Gamma_7$ transition is favored in E $\perp$ c configuration, while $\Gamma_7 \rightarrow \Gamma_9$ transition involving states from the B valence band are allowed in E || c configuration. However the coupling of the exciton-polariton branches leads to a relaxation of these selection rules, and the appearance of previously forbidden transitions.

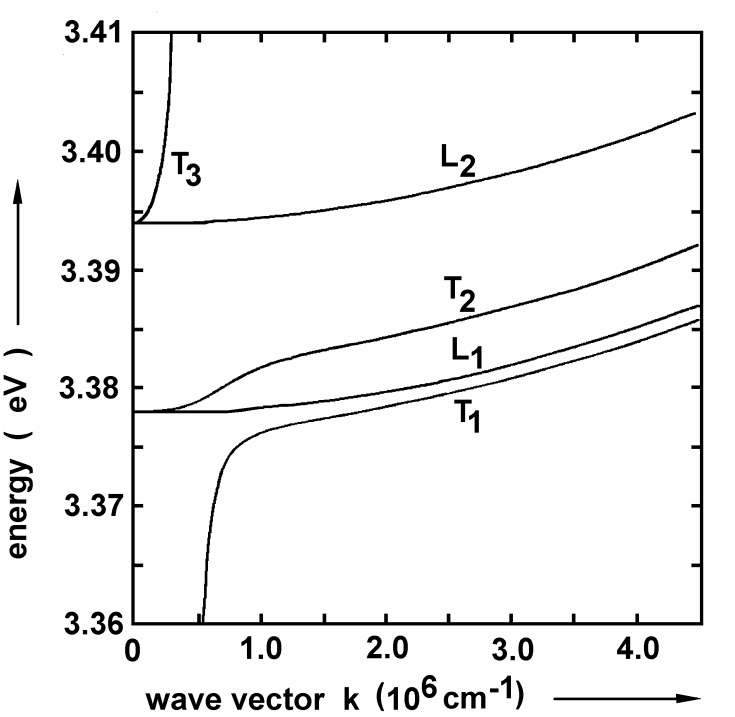

Fig. 3. Dispersion relation of exciton-polaritons in ZnO. The various transversal (T1, T2, T3) and longitudinal (L1, L2) exciton-polariton dispersion curves are shown for a temperature of 2 K.

One possibility to determine the symmetry of the valence bands and the band ordering are magneto-optical studies. This technique is not only a powerful and versatile method to elucidate the nature of exciton binding centers involved in optical transitions with respect to their charge state (neutral or ionized) and impurity type (donor or acceptor) [24] but also provides information on the symmetry of the hole states involved in the bound exciton complexes. Of particular interests are angular dependent measurements, where the angle between the crystal c-axis and the orientation of the magnetic field is varied. Theoretical consideration show that the splitting of the bound exciton line by the Zeeman effect for arbitrary angles between the principal axis and the direction of the external magnetic field is strongly effected by the symmetry of the hole states involved in the bound exciton complex.

The knowledge of the valence band ordering is of particular interest, since the investigated epilayers are often subject to residual strain. Gil et al. [25] have shown that the influence of strain-field effects can reverse the ordering of the valence bands, thus leading to reversed peak positions for the transitions of the top most A and B valence band. In order to clarify this issue, angular dependent magneto optical photoluminescence measurements were performed.

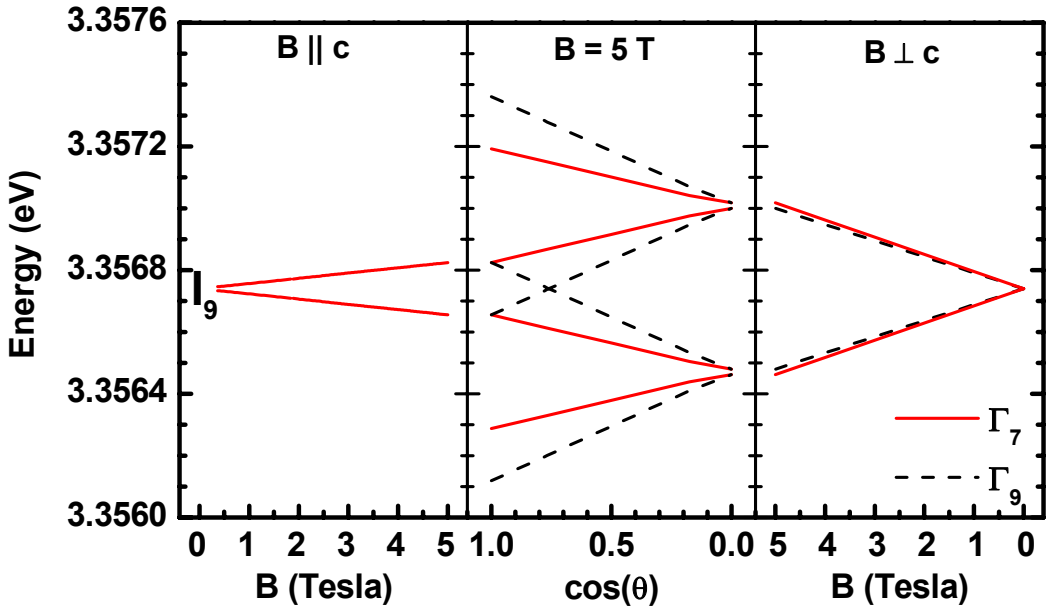

Fig. 4. Calculated Zeeman splitting of the I_9 bound exciton line for holes with Γ_7 (solid lines) or Γ_9 (dashed lines) symmetry. The splitting as a function of the applied magnetic field is given for B ∥ c (left) and B $\perp$ c (right), as well as for arbitrary angles at a constant magnetic field strength of 5 Tesla (middle).

The Zeeman splitting of the I_9 donor bound exciton line, which has been attributed to an indium impurity [26, 27] is depicted in Fig. 4. The splitting of the transition lines has been calculated for excitonic complexes involving hole states originating from valence bands with either Γ_7 (solid lines) or Γ_9 (dashed lines) symmetry [28]. The theoretical calculations have been performed using the linearized muffin tin orbital method with local density approximation including spin-orbit coupling. Evidently, the most significant difference in the splitting for Γ_7 and Γ_9 symmetry appears in the angular dependent plot. While the fourfold splitting of the Zeeman components is considerably smaller for Γ_7 symmetry, the calculations predict a larger splitting which leads to a crossing of the two inner Zeeman components for excitons involving hole state with Γ_9 symmetry. However, this crossing has never been observed for an exciton involving a hole from the A valence band. In fact, theoretical and experimental results provide strong evidence [28, 29] that the valence band ordering is indeed Γ_7, Γ_9, Γ_7 as originally proposed by Thomas.

3. HOMOEPITAXIAL GROWTH OF ZINC OXIDE LAYERS

We used a micro Raman setup to obtain information on a micrometer scale about several ZnO samples grown on ZnO templates. Our measurements were carried out at room-temperature with a DILOR XY 800 triple-grating Raman spectrometer (1800 l/mm) and a charge-coupled device (CCD) camera working at liquid nitrogen temperature as detector. The samples were excited either parallel (in-plane) or perpendicular (on-plane) to the surface using an Ar^+ - Kr^+ mixed-gas laser. The micro optics (100 times magnified) focused the laser on a point spot of about 0.5 µm diameter and collected the scattered light in backscattering geometry. This corresponds to an *x(...)*$\underline{x}$ configuration for in-plane excitation and a *z(...)*$\underline{z}$ configuration for on-plane excitation according to the well-known *Porto*-notation: the samples *c*-axis is parallel to the *z*-direction and the *x*- and *y*-axes are perpendicular to each other and the *z*-axis but arbitrary in the *z*-plane.

Under equilibrium conditions ZnO crystallizes in the wurtzite structure and belongs to the point group C_{6v} (6mm) with Raman-active modes permitted in backscattering geometries as listed in Table 1.

Table. 1. First-order Raman modes in ZnO for different backscattering geometries

Configuration	Permitted Raman modes
$z(xx)z$	E_2(low, high), A_1(LO)
$z(yx)\underline{z}$	E_2(low, high)
$x(zz)\underline{x}$	A_1(TO)
$x(yy)\underline{x}$	A_1(TO), E_2(low, high)
$x(yz)\underline{x}$	E_1(TO)

The corresponding Raman spectra are shown in Fig.5. The Raman modes and scattering geometries are indicated. These measurements were carried out on a nominally undoped ZnO single crystal with almost perfect orientated axes. The common feature of the on-plane spectra (Fig. 5a) is the absence of the TO modes. Among the in-plane spectra (Fig. 5b) the $x(zz)\underline{x}$ configuration should be noted because of the total disappearance of the E_2 modes. It is the only backscattering configuration not showing E_2 lines despite the fact that they are also 'forbidden' in $x(yz)\underline{x}$ geometry. In fact they seem to occur in this configuration irrespective of the crystal quality or the precision of the polarization. An accurate explanation of this matter is a subject for further investigations.

Structures labeled with an asterisk are due to multiphonon scattering [7]. The E_1(LO) mode is actually not allowed in any backscattering geometry but visible in the spectrum taken in $x(zz)\underline{x}$ configuration. It originates probably from scattering processes permitted via deformation potential and particularly the Fröhlich interaction, described by two terms which represent the intra- and interband scattering. A detailed discussion on how they can contribute to a 'forbidden' LO-scattering is given in [30]. Alternatively it might be caused by rectangle scattering induced by back reflections which occur due to the fact that the sample is transparent to the laser beam.

To reemphasize one should note that the $x(zz)\underline{x}$ configuration is the most sensitive tool to prove the crystal orientation of a sample. The appearance of E_2 lines indicates a tilt of the *c*-axis even in high-quality material. The $x(yy)\underline{x}$ geometry in the case of in-plane and the $z(\ldots)\underline{z}$ setups in the case of on-plane, respectively, are suitable to probe the strain properties because of the distinct occurrence of the E_2 modes. They are, other than the TO and LO vibrations, non-polar and thus not affected by free carriers or internal electric fields but only by stress.

3.1 Undoped ZnO/ZnO samples

We investigated two types of nominally undoped ZnO layers and compared the results to those presented above. Both were grown by Chemical Vapor Deposition (CVD) on ZnO templates. The samples differ as they are partly grown on the oxygen-terminated surface of the ZnO template and partly on the Zn face. Both cases produce samples which are compressively strained and both exhibit a sudden but incomplete relaxation in a depth of around 5 to 7 µm. This relaxation is more pronounced in layers grown on O-face. Both CVD-grown ZnO layers are much thinner, we estimate their thickness to be approximately at the most 1 µm. Consequently, this rapid change in strain properties occurs in the template and not in the CVD-grown layers. Our investigation on an untreated substrate revealed no evidence for this behavior. It was also found to be compressively strained with a homogenous distribution over the whole sample. No abrupt changes were visible, neither near the surfaces nor in the deeper regions. We assume the growth process being the origin for this inconsistent behavior. The ZnO templates need to be prepared by a consecutive annealing procedure to get a certain surface roughness that is essential to start the growth process. This might cause a change only in near-surface regions of the sample which is 'frozen' due to the subsequent growth of the CVD layer.

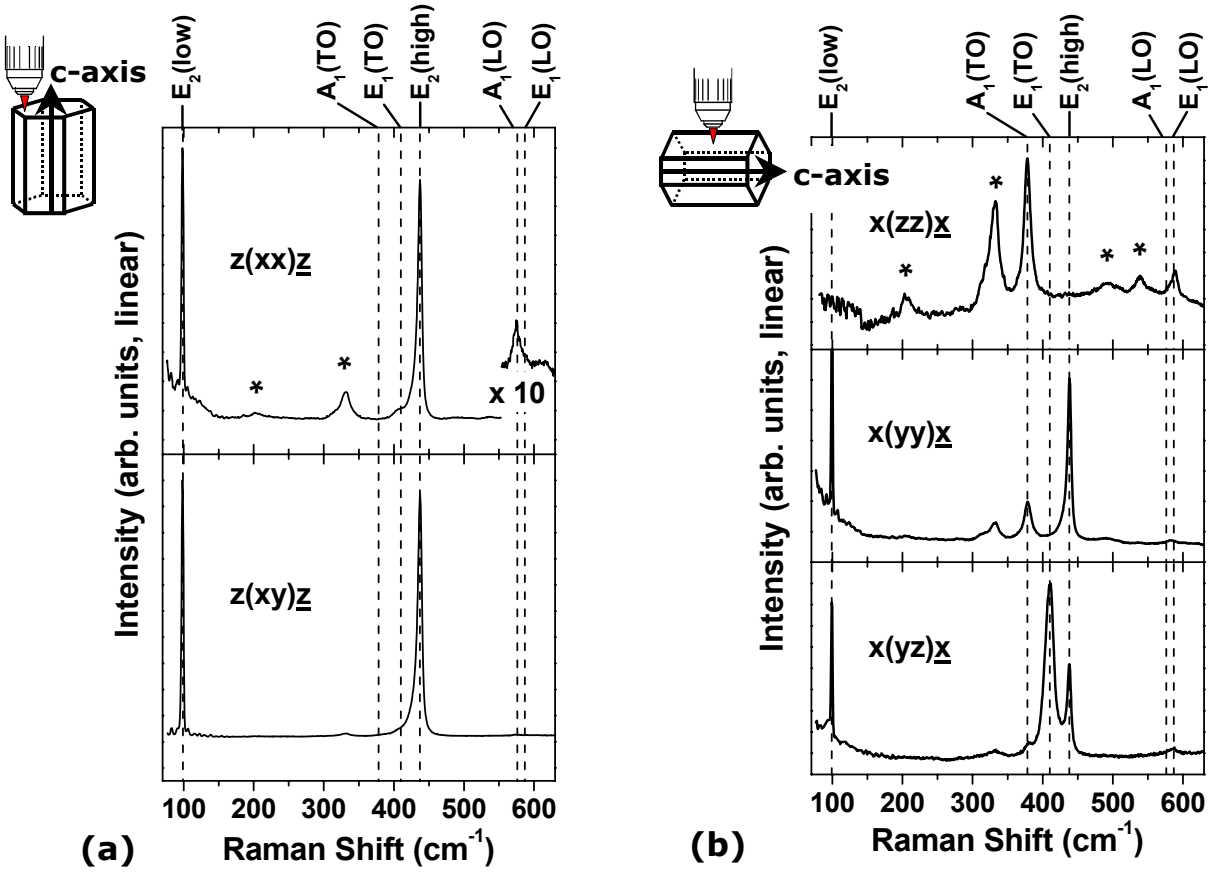

Fig. 5. Room-temperature Raman spectra of a ZnO single crystal taken in different (a) on-plane and (b) in-plane scattering configurations as depicted. Peaks labeled with an asterisk originate from multiphonon scattering.

Aside from the change in strain properties we found regions with non perfect crystal symmetry or orientation in the mentioned x(*zz*)x configuration (Fig. 6). Only the spectral range of the A_1(TO) and E_2(high) are displayed for clarity. The E_2 line actually forbidden in this geometry appears distinct and comparable in intensity to the allowed TO mode. The reason might be a tilt of the *c*-axis or weakened selection rules due to crystal perturbations. We observed such behavior sporadically in both ZnO layers being grown on Zn- or O-face but not in the native template. The lowering of the symmetry or rather a tilt of the *c*-axis does not coincidence with poor crystal quality. In contrary we observed narrow Raman lines comparable to those of high-quality single crystals. The Raman results seem to indicate that the growth on the Zn-terminated surface of the ZnO template has produced a slightly better crystal quality than the growth on O-face. To draw a final conclusion more research has to be done.

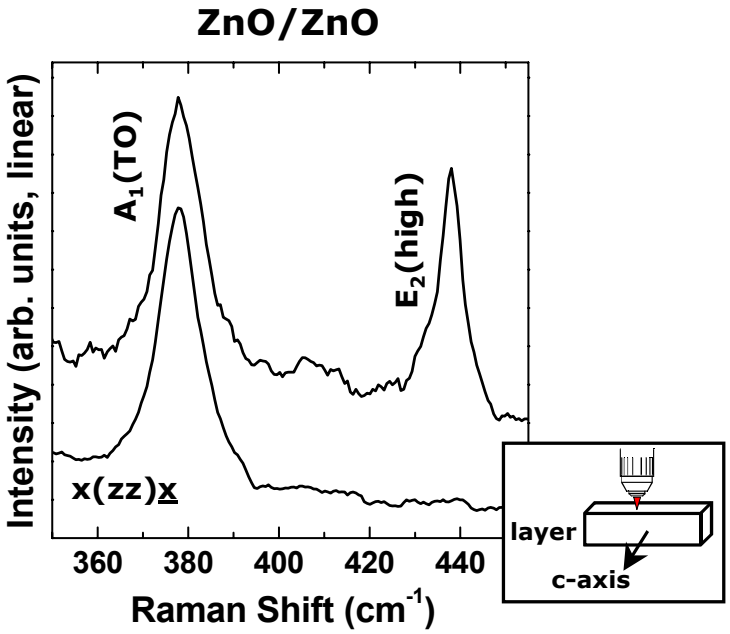

Fig. 6. Room-temperature Raman spectra taken in different depth of an undoped ZnO layer grown on ZnO template. The lower curve shows the shape expected in $x(zz)\underline{x}$ configuration (no E_2-mode), the upper curve illustrates a crystal perturbation (appearance of the forbidden E_2 mode).

3.2 ZnO:Li/ZnO properties

Shallow impurity levels are predicted for ZnO doped with group I elements [31]. However, different theoretical and experimental conclusions narrowing the possibility of lithium substituted for zinc (Li_{Zn}) that led to an acceptor state in p-type material were reported [32-34]. Recent experimental results indicate that the formation of shallow or deep lithium acceptor levels strongly depends on the growth or diffusion temperature [35]. Here we focus on the lattice dynamics of Li-doped ZnO with respect to crystal quality and orientation as well as strain properties. The sample under investigation is CVD-grown on ZnO substrate, which is not identically to those used for the growth of the above described undoped layers. In contrast to the previous the template of this sample is almost relaxed. The deposited ZnO layer is thus not compressively strained but still not fully relaxed. We found it to be slightly tensile strained and we obtained changes in the strain behavior similar to the undoped material but not as rapid as observed before. From the surface of the CVD-grown layer towards the substrate the tensile strain decreases until reaching a depth of 5 µm. Within the next 5 µm, we observed an increasing tensile strain and for even larger depth a switchback towards the relaxed state. Over the rest of the sample no more changes are visible.

Although the change in strain properties arises continuously, we found a radical change of the Raman spectra over an interval of only 0.25 µm. It occurs in a depth of 5 µm and thus at the same depth when the tensile strain increases again. Fig. 7 displays the spectra taken in a depth of 5 µm and 5.25 µm, respectively. From the shape expected in $x(yz)\underline{x}$ configuration we found a switch to a curve looking like a $z(yx)\underline{z}$ geometry . This means that the *c*-axis has rotated by 90° forming a separated growth domain. With increasing depth the Raman spectra change back to the initial $x(yz)\underline{x}$ shape. The same procedure was observed in the very near surface region. Despite taking Raman spectra in an in-plane configuration, $x(yz)\underline{x}$, the shape looks first like an on-plane geometry, namely $z(yx)\underline{z}$. Along the next 5 µm further in direction towards the substrate the curves change gradually to the expected $x(yz)\underline{x}$ figure.

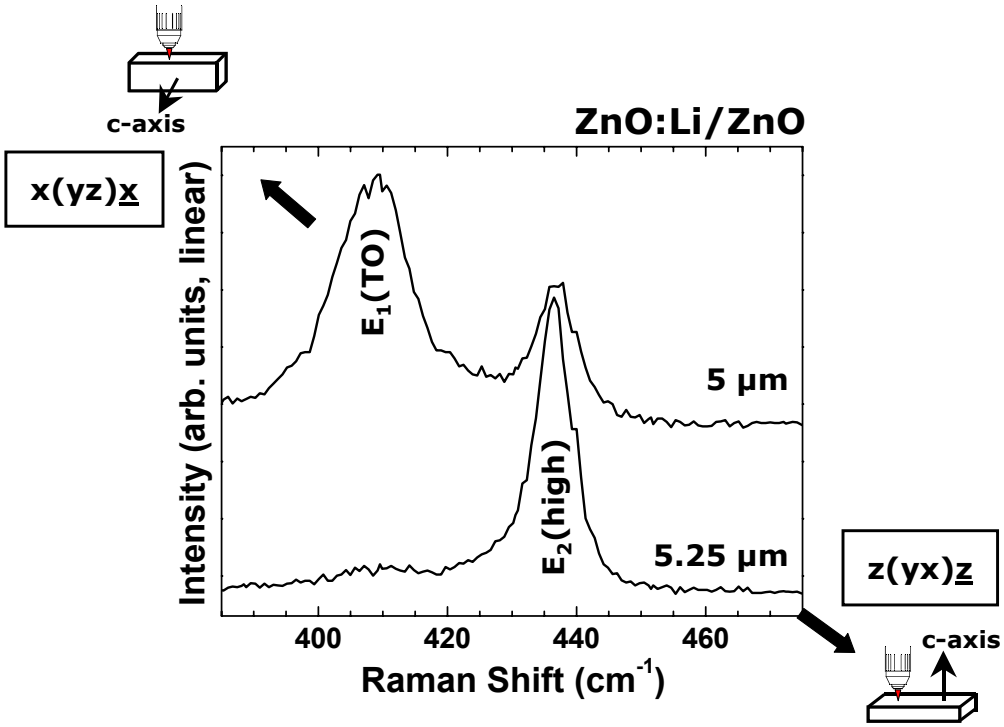

Fig. 7. Raman spectra of Li-doped ZnO grown on ZnO substrate. The spectra were taken at intervals of only 0.25 µm showing a switch between an in-plane (upper curve) and an on-plane (lower curve) configuration.

Thus we differentiate between three growth domains: domain 1 exists from the surface of the CVD-grown ZnO layer to a depth of 5 µm, domain 2 ranges from 5 to 10 µm. Both exhibit a change from an on-plane to an in-plane shape, accompanied by a modification of the strain properties. The final domain 3 remains almost relaxed and the Raman spectra exhibit the shape as expected in $x(yz)\underline{x}$ configuration.

4. RESONANT RAMAN SCATTERING

In the present study, we present photoluminescence (PL) and resonant Raman scattering (RRS) measurements of high-quality CVD grown ZnO. To obtain temperature independent results we use a frequency doubled titan-sapphire laser that provided a continuous tuning of the emission energy, hence permitting the variation of the excitation wavelength in the range of 350 to 400 nm. The laser wavelength could be calibrated with an accuracy of approximately 0.1 nm. By adjusting the laser energy to the free and bound exciton energies of ZnO, we obtained resonant excitations of the various excitonic complexes. We applied a detailed and comprehensive analysis of the resonance behavior and the influence of exciton-phonon interactions, such as the deformation potential and the Fröhlich interaction. Similar studies have already been performed in GaN [36].

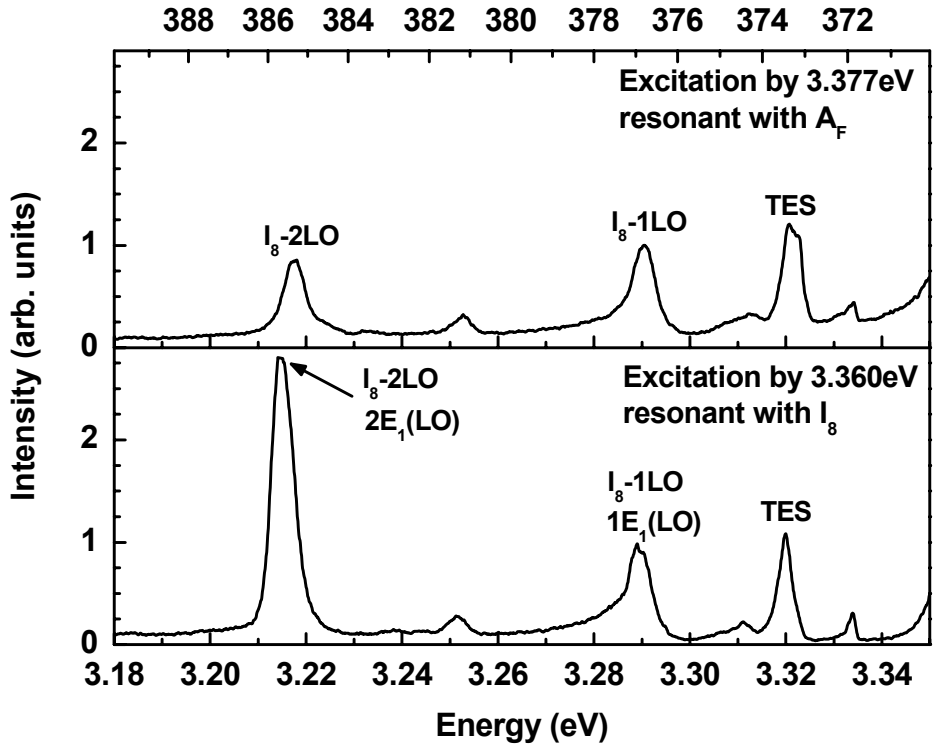

Fig. 8. PL and Raman spectra of CVD grown ZnO at 1.8 Kelvin for two different laser excitation energies. Top graph: Excitation at 3.377eV (in resonance with the A free exciton A_F), bottom graph: excitation at 3.360eV (in resonance with the donor bound exciton complex I_8)

The PL and Raman spectra at 1.8 Kelvin were acquired at different excitation energies in the range of 3.18eV to 3.35eV and are presented in Fig. 8. The near band-edge PL spectrum demonstrates that the I_8 bound exciton complex - which has been attributed to a gallium donor complex [26, 37] - is the dominant excitonic transition in the sample under investigation (not shown). The upper graph in Fig. 8 displays the spectrum for an excitation energy of 3.377eV. This energy is in resonance with the A_F exciton. Aside from the two-electron satellite (TES) and the structural defect line at 3.333eV [26], the 1LO and 2LO phonon replica of the dominant I_8 bound exciton line are clearly apparent. In order to facilitate the comparison of intensities, both spectra have been normalized to the I_8-1LO peak. The intensity of the I_8-2LO line in the upper graph is slightly smaller (0.84) compared to the intensity of the I_8-1LO line. Such a behavior is also expected for a phonon replica in non-resonant excitation.

However, in the second spectra with resonant excitation at the I_8 bound exciton energy, the intensity of the 2LO line (2.80) compared to the 1LO line is significantly increased. It is important to distinguish between the two different physical processes involved. These are (i) the non-coherent luminescence process resulting from the phonon replica of the I_8-bound exciton with a typical spacing of the LO phonon energy of 72.2meV and (ii) the coherent Raman process of the $2E_1$(LO) mode, which is greatly enhanced due to the Fröhlich interaction. The latter is solely responsible for the observed resonance enhancement. In contrast to other non-polar modes which interact only via the deformation potential, the polar LO modes are also subject to Fröhlich interaction. Hence, the increased intensity towards the bound exciton resonance due to the Coulomb interaction between the longitudinal electric field of the phonons and the charges of the excitons implies that the scattering process is mediated via a real excitonic state.

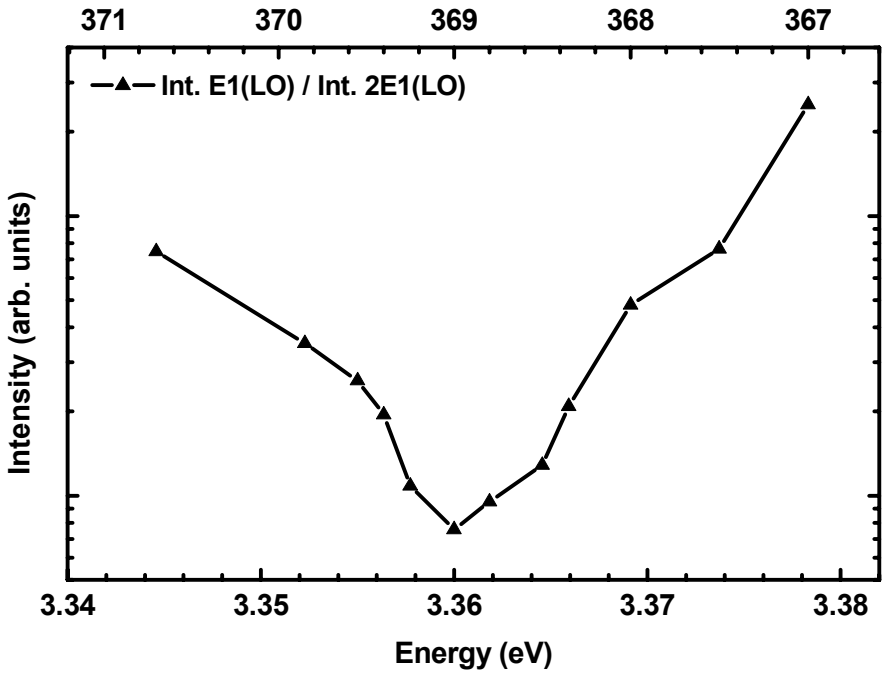

Fig. 9. Intensity ratio of the E_1(LO) Raman mode divided by the intensity of the $2E_1$(LO) Raman peak for different excitation energies (displayed on a logarithmic scale). The solid lines are a guide to the eye only.

In order to obtain the resonance profile of the $2E_1$(LO) Raman mode, multiple spectra with different excitation energies in the range of 3.34eV to 3.38eV were recorded. For each spectrum the intensities of the E_1(LO) and $2E_1$(LO) line were determined. Fig. 9 shows the intensity ratio of these two lines as a function of the laser excitation energy. Apparently, there is a minimum (largest enhancement of the $2E_1$(LO) compared to the E_1(LO) mode) for an excitation energy of 3.360eV, which is consistent with the energy of the I_8 bound exciton complex. The resonance profile supports our assignment, that the resonance enhancement is strongly dependent on the existence of excitonic complexes. The results of additional time resolved studies indicate that the life time of the Raman mode - which is usually of similar magnitude to those of the exciting laser – is increased due to the scattering via a real excitonic state rather than a virtual state with the Fröhlich interaction being the determining exciton-phonon interaction.

5. CONCLUSION

In summary, we have derived the exciton-polariton dispersion from angular dependent reflection spectra, revealing a longitudinal-transverse splitting of 3.9 and 9.0eV for the A and B exciton-polaritons, respectively. Magneto optical studies confirmed that the valence band ordering is Γ_7, Γ_9, Γ_7. The strain properties in homoepitaxially grown ZnO layers were found to be primarily determined by the template. We observed in parts strong gradients accompanied by crystal perturbations or even the existence of separated growth domains in the samples. Finally, resonant Raman spectroscopy showed a strong enhancement of the $2E_1$(LO) mode for an excitation energy in resonance with the dominant bound exciton complex.

REFERENCES

1. W. Y. Liang and A. D. Yoffe "Transmission spectra of ZnO single crystals", *Phys. Rev. Lett.* 20, 59 (1968).
2. D. C. Reynolds, D. C. Look, B. Jogai, C. W. Litton, G. Cantwell, and W. C. Harsch, "Valence-band ordering in ZnO", *Phys. Rev. B* 60, 2340 (1999).
3. S. F. Chichibu, A. Uedono, A. Tsukazaki, T. Onuma, M. Zamfirescu, A. Ohtomo, A. Kavokin, G. Cantwell, C. W. Litton, T. Sota, and M. Kawasaki, "Exciton-polariton spectra and limiting factors for room temperature photoluminescence efficiency in ZnO, *Semicond. Sci. Technol.* 20, S67-S77 (2005).
4. M. Zamfirescu, A. Kavokin, B. Gil, G. Malpuech, M. Kaliteevski, „ZnO as a material mostly adapted for the realization of room-temperature polariton lasers", *Phys. Rev. B* 65, 161205(R) (2002).
5. R. Loudon, *Proc. Phys. Soc. Lond.* 82, 393 (1963).
6. A. K. Ganguly and J. L. Birman, "Theory of Lattice Raman Scattering in Insulators" *Phys. Rev.* 162, 806 (1967)
7. J. M. Calleja and M. Cardona, "Resonant Raman scattering in ZnO", *Phys. Rev.* 16(8), 3753-3761 (1977).
8. R. C. C. Leite and S. P. S. Porto, "Enhancement of Raman Cross Section in CdS due to Resonant Absorption" *Phys. Rev. Lett.* 17, 10 (1966).
9. T. C. Damen and J. Shah, "Bound Exciton Resonance in Raman Cross Section in CdS", *Phys. Rev. Lett.* 27, 1506 (1971).
10. T. C. Damen and J. F. Scott, "Antiresonance of Raman Cross Section for Nonpolar Phonons in CdS", *Sol. Stat. Comm.* 9, 383, (1971).
11. R. Baumert, I. Broser, J. Gutowski, and A. Hoffmann, "Forbidden Luminescence and Resonance Raman Scattering of Bound Exciton States in CdS", *Phys. Stat. Sol (b)*, 116, 261 (1983).
12. J. F. Scott, "UV Resonant Raman Scattering in ZnO", Phys. Rev. B, 2, 1209 (1970).
13. X. T. Zhang, Y. C. Liu, Z. Z. Zhi, J. Y. Zhang, Y. M. Lu, D. Z. Shen, W. Xu, G. Z. Zhong, X. W. Fan, and X. G. Kong, "Resonant Raman scattering and photoluminescence from high-quality nanocrystalline ZnO thin films prepared by thermal oxidation of ZnS thin films", *J. Phys. D: Appl. Phys.* 34, 3430 (2001) .
14. B. Kumar, H. Gong, S. Y. Chow, S. Tripathy, and Y. Hua, "Photoluminescence and multiphonon resonant Raman scattering in low-temperature grown ZnO nanostructures", *Appl. Phys. Lett.* 89, 071922 (2006).
15. V. V. Zalamai, V. V. Ursaki, E. V. Rusu, P. Arabadji, I. M. Tiginyanu, and L. Sirbu, "Photoluminescence and resonant Raman scattering in highly conductive ZnO layers", *Appl. Phys. Lett.* 84, 5168 (2004).
16. V. V. Ursaki, I. M. Tinginyanu, V. V. Zalamai, E. V. Ruso, G. A. Emelchenko, V. M. Masalov, and E. N. Samarov, "Multiphonon resonant Raman scattering in ZnO crystals and nanostructured layers", *Phys. Rev. B* 70, 155204 (2004).
17. D. G. Thomas, "The exciton spectrum of zinc oxide", *J. Phys. Chem. Solids* 15, 86 (1960).
18. W. Y. Liang and A. D. Yoffe, "Transmission spectra of ZnO single crystals", *Phys. Rev. Lett.* 20, 59 (1968).
19. D. C. Reynolds, C. W. Litton, and T. C. Collins, "Zeeman effects in the edge emission and absorption of ZnO", *Phys. Rev.* 140, 1726 (1965).
20. Y. S. Park, C. W. Litton, T. C. Collins, and D. C. Reynolds, "Exciton spectrum of ZnO", *Phys. Rev.* 143, 512 (1966).
21. M. Cardona, "Optical properties of the silver and cuprous halides", *Phys. Rev.* 129, 69 (1963).
22. K. Shindo, A. Morita, and H. Kamimura, "Spin-orbit coupling in ionic crystals with zincblende and wurtzite structures", *J. Phys. Soc. Jpn.* 20, 2054 (1965).
23. R. T. Girard, O. Tjernberg, G. Chiaia, S. Sönderholm, U. O. Karsson, C. Wigren, H. Nylen, and I. Lindau, "Electronic structure of ZnO(0001) studied by angle-resolved photoelectron spectroscopy", *Surf. Sci.* 373, 409 (1997).
24. D. G. Thomas and J. J. Hopfield, "Bound exciton complexes", *Phys. Rev. Lett.* 7, 316 (1961).
25. G. Gil, A. Lusson, V. Sallet, S.-A. Said-Hassani, R. Triboulet, and P. Bigenwald, "Strain-fields effects and reversal of the nature of the fundamental valence band of ZnO epilayers", *Jpn. J. Appl. Phys.* 40, 1089 (2001).
26. B. K. Meyer, H. Alves, D. M. Hofmann, W. Kriegseis, D. Forster, F. Bertram, J. Christen, A. Hoffmann, M. Straßburg, M. Dworzak, U. Haboeck, and A. V. Rodina "Bound exciton and donor-acceptor pair recombinations in ZnO", *Phys. Stat. Sol. (b)* 241, 231 (2004).

27. S. Müller. D. Stichtenoth, M. Uhrmacher, H. Hofsäss, C. Ronning, and J. Röder, „Unambiguous identification of the PL-I_9 line in zinc oxide", *Appl. Phys. Lett.* 90, 012107 (2007).
28. A. V. Rodina, M. Strassburg, M. Dworzak, U. Haboeck, A. Hoffmann, A. Zeuner, H. R. Alves, D.M. Hofmann, and B.K. Meyer, "Magneto-optical properties of bound excitons in ZnO", *Phys. Rev. B* 69, 125 206 (2004).
29. W. R. L. Lambrecht, A. V. Rodina, S. Limpijumnong, B. Segall, and B. K. Meyer, "Valence-band ordering and magneto-optic exciton fine structure in ZnO", *Phys. Rev. B* 65, 075 207 (2002).
30. M. Cardona, *Light Scattering in Solids II*, M. Cardona and G. Güntherodt (ed.), Topics Appl. Phys. 50, Springer Berlin, 1982.
31. C. H. Park, S. B. Zhang, and S.-H. Wei, "Origin of p-type doping difficulty in ZnO: The impurity perspective", *Phys. Rev. B* 66, 073202 (2002).
32. P. H. Kasai, "Electron spin resonance studies of donors and acceptors in ZnO" Phys. Rev. 130, 989 (1963).
33. E. Tomzig and R. Helbig, "Band-edge emission in ZnO", *J. Lum.* 14, 403 (1976).
34. M. G. Wardle, J. P. Goss, and P. R. Briddon, "Theory of Li in ZnO: A limitation for Li-based p-type doping", *Phys. Rev. B* 71, 155205 (2005).
35. B.K. Meyer, N. Volbers, A. Zeuner, S. Lautenschläger, J. Sann, A. Hoffmann, and U. Haboeck, "Group I elements in ZnO", *Mater. Res. Soc. Symp. Proc.* 891, EE10-24.1 (2006).
36. A. Kaschner, A. Hoffmann, and C. Thomsen, "Resonant Raman scattering on free and bound excitons in GaN", *Appl. Phys. Lett.* 64, 165314 (2001).
37. K. Johnston, M. O. Henry, D. McCabe, E. McGlynn, M. Dietrich, E. Alves, and M. Xia, "Identification of donor-related impurities in ZnO using photoluminescence and radiotracer techniques", *Phys. Rev. B* 73, 165212 (2006).